Contact stress analysis of lightly compressed thin films: Modeling and experimentation

Elon J. Terrell,[1] M. Aslam Kabir,[2] and C. Fred Higgs III[2,a)]
[1]*Department of Mechanical Engineering, Columbia University, New York, New York 10027, USA*
[2]*Department of Mechanical Engineering, Carnegie Mellon University, Pittsburgh, Pennsylvania 15213, USA*

(Received 19 March 2009; accepted 6 May 2009; published online 22 June 2009)

Although a number of models have been developed to describe the contact between nominally smooth surfaces, very few of these models have been validated with experiment. Therefore, in this study, an asperity-scale experimental contact measurement was conducted and compared to the predictions of two contact models. The experimental component of this study involved a flat diamond punch tip on a nanoindenter, which was used to compress a thin film that was lithographically patterned into isolated raised squares. This experimental method was developed in order to measure the predominantly elastic load response of the surface asperities on one of the isolated raised topography islands. The experimental measurements were compared to the predicted load responses of an existing analytical contact model as well as a finite element contact model that incorporated the topography of the raised island into its formulation. The predictions of both the models were shown to have reasonable agreement with the experimental data. The modeling results were also used to provide greater depth of insight into the physics of the flat punch compression.
 [DOI: 10.1063/1.3143893]

I. INTRODUCTION

The study of asperity interaction between nominally flat surfaces is of great importance in tribology and contact mechanics since both friction and wear take place on the asperity scale. One area of contact mechanics that has garnered attention has been the contact of real surfaces that are very smooth or lightly loaded, where the deformation is predominantly elastic. This fundamental problem has implications on the analysis of emerging nanoscale electromechanical systems,[1] micro-scale electromechanical systems,[1–3] chemical mechanical polishing,[4–7] and hard disk drive sliders,[8–10] where the participating surfaces are smooth and the resulting loads are of the order of μN. Numerous modeling treatments have been employed for studying rough surfaces in contact, including statistical, multiscale,[11–13] finite element, and deterministic approaches. Additional studies have used numerical analysis to analyze the subsurface stresses in contacting rough surfaces.[14–16]

Statistical approaches to modeling surfaces in contact have followed the seminal work of Greenwood–Williamson (GW), who assumed that a surface topography could be described as being composed of hemispherical asperities with constant radii and randomly varying heights.[17] This work has led to a number of other studies[6,18–20] that also represented contacting surfaces as random height distribution functions.

Finite element method (FEM) analysis has also been a powerful tool for providing information on asperity contact interactions.[18–20] Results from FEM simulations have led to closed form equations for load-interference response and real contact area.[21] FEM simulations have advanced the fields of contact mechanics and tribology greatly due to their ability to incorporate surfaces with complex geometries and perform rigorous contact modeling. Commercial FEM simulations can also handle databased treatment of topography data[22] in the same manner as deterministic approaches, yet are computationally expensive.

In this study, an experiment was conducted where a rough thin film sample surface was experimentally measured using contact profilometry and then uniformly compressed by a flat-face diamond tip attached to a nanoindenter. The contact behavior was then modeled using both a FEM approach and a statistical contact model from a Kadin *et al.*[23] Both the modeling and experimental approaches were used to analyze the elastic-plastic contact between a relatively rough thin film sample surface and a nominally smooth flat plane.

II. SAMPLE SURFACE PREPARATION AND CHARACTERIZATION

The sample in this study consisted of SU-8 epoxy material lithographically patterned into an array of raised square regions on a silicon substrate. The sample was prepared by spreading a blanket uniform layer of negative SU-8 photoresist onto the substrate and hard baking it. After baking, the photoresist was exposed to ultraviolet light through a mask of transparent squares and then developed, leaving only the array of raised squares.

Each of the raised square regions had random roughness due to the SU-8 deposition process. Elastic modulus and hardness measurements were first taken for the SU-8 film using a series of indents with a nanoindenter (Hysitron TriboIndenter) with a Berkovich tip. Table I shows the resulting parameter measurements that were used as inputs to the analytical and FEM contact models.

a)Author to whom correspondence should be addressed. Electronic mail: higgs@andrew.cmu.edu.

TABLE I. Material properties that were specified for the contact models.

Parameter	Source	Value
Elastic modulus of sample, E_{sample}	Measured in this study	7.64 ± 0.37 GPa
Hardness of sample, H_{sample}	Measured in this study	0.462 ± 0.026 GPa
Yield strength of sample, Y_{sample}	Measured in this study	0.165 ± 0.0093 GPa
Poisson's ratio of sample, ν_{sample}	Kim *et al.*[a]	0.22
Elastic modulus of flat tip, E_{flat}	Hysitron[b]	1140 GPa
Poisson's ratio of flat tip, ν_{flat}	Hysitron[b]	0.07

[a]Reference 24.
[b]Reference 25.

After measuring the film properties, one of the raised squares was isolated for contact mechanics analysis, as shown in Fig. 1. The isolation of an individual raised square allowed for a consistent surface topography for both modeling and experimentation.

The square that was targeted for this study had nominal (prelithographic) dimensions of $R=25$ μm by $S=25$ μm and a measured average thickness of $t=6.3$ μm. The topography of the square was measured using contact profilometry, which measured the surface topography over a square area of $R'=60$ μm $\times S'=60$ μm. A three-dimensional raster scan of the raised surface is shown in Fig. 2.

III. EXPERIMENTAL CONTACT MEASUREMENTS

In order to provide an experimental basis for comparing with the FEM and analytical modeling approaches, the square sample underwent compression testing using a large flat diamond tip that was attached to the nanoindenter. The flat section of the tip was 100 μm in diameter and large enough to completely encompass the 25×25 μm^2 square sample. A scanning electron microscope (SEM) image of the tip is shown in Fig. 3. It must be noted that the roughness of the face of the tip was specified to be less than 10 nm according to the manufacturer. For the purposes of this study, the diamond surface was assumed to be a "smooth" flat plane relative to the rougher thin film sample, thus making the experiment into a "flat punch contacting a rough surface" phenomenon that can be predicted by the FEM and analytical contact models. After ensuring that the flat tip was correctly positioned over the sample, a load-unload compression test was performed with a peak load of $W_{max}=1000$ μN, while the normal force-interference response of the surface was measured *in situ*.

The compression test, which was load-controlled, was conducted with a loading rate of 50 μN/s and an unloading rate of 20 μN/s. It was believed that these load/unload rates were slow enough and the peak load was sufficiently light to assume quasistatic elastic-plastic compression of the sample. It must be noted that the zero-interference point ($\omega=0$) was marked at the place where the load response was equal to $W=25$ μN, which is the minimum applied force that can be resolved by the nanoindenter.[25] The silicon substrate was assumed to experience a negligible amount of bending and compression during the contact measurements.

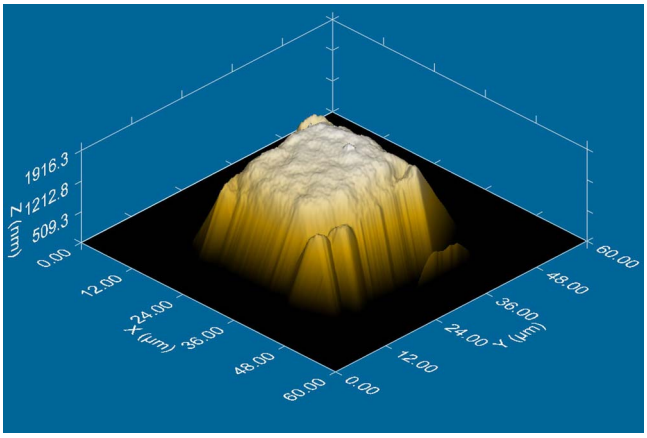

FIG. 2. (Color online) Three-dimensional plot of surface topography of the raised square region that was analyzed.

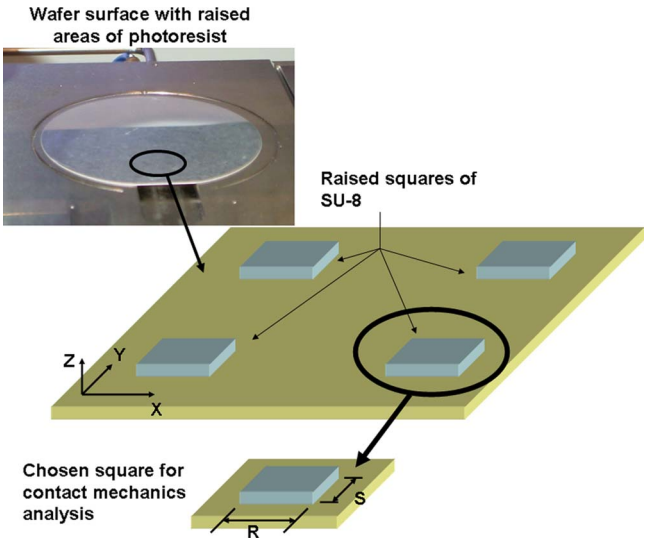

FIG. 1. (Color online) Diagrams of wafer surface and raised squares of SU-8 film.

IV. EXTRACTION OF CONTACT PARAMETERS FOR MODELING COMPARISON

The required contact modeling parameters were extracted using the measured surface topography and material

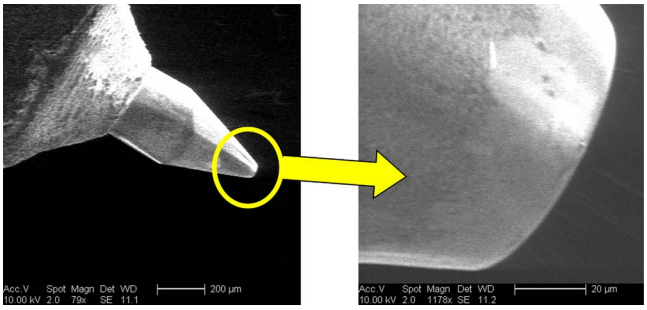

FIG. 3. (Color online) SEM images of (a) flat punch nanoindentation tip and (b) the leading edge of the flat punch tip.

properties from this study. A variation in the formulation presented by McCool[26] was employed in order to calculate the average asperity radius of curvature R_{asp}, asperity density η, and standard deviation of asperity heights σ_s for the contacting region of the topography. From the measured surface topography $z(x,y)$, surface parameters were calculated as follows:

$$m0 = \mathrm{AVG}[z^2(x,y)] = 0.002\ 132\ 79\ \mu\mathrm{m}^2, \tag{1}$$

$$m2 = \left(\mathrm{AVG}\left[\left(\frac{\partial z(x,y)}{\partial x}\right)^2\right] + \mathrm{AVG}\left[\left(\frac{\partial z(x,y)}{\partial y}\right)^2\right]\right)/2 = 0.002\ 300\ 23, \tag{2}$$

$$m4 = \left(\mathrm{AVG}\left[\left(\frac{\partial^2 z(x,y)}{\partial x^2}\right)^2\right] + \mathrm{AVG}\left[\left(\frac{\partial^2 z(x,y)}{\partial y^2}\right)^2\right]\right)/2 = 0.017\ 103\ 6\ \mu\mathrm{m}^{-2}, \tag{3}$$

where AVG[] is the mean value of a prescribed function and $m0$, $m2$, and $m4$ are the zeroth, second, and fourth spectral moments of the surface topography, respectively. The asperity radius of curvature R_{asp} and standard deviation of summit heights σ_s were then calculated as follows:

$$R_{asp} = 0.375\sqrt{\frac{\pi}{m4}} = 5.08\ \ \mu\mathrm{m}, \tag{4}$$

$$\sigma_s = \left(\sqrt{1 - \frac{0.8968(m2)^2}{m0m4}}\right)\sqrt{m0} = 0.0431\ \ \mu\mathrm{m}. \tag{5}$$

After extracting these parameters, the critical interference for elastic-plastic deformation, originally presented by Chang *et al.*,[27] was calculated as follows:

$$\omega_c = \left(\frac{\pi K H_{sample}}{2E'}\right)^2 R_{asp} = 0.0125\ \ \mu\mathrm{m}, \tag{6}$$

where E' is the composite elastic modulus given by

$$E' = \left(\frac{1-\nu_{sample}{}^2}{E_{sample}} + \frac{1-\nu_{flat}{}^2}{E_{flat}}\right)^{-1} = 8.31\ \ \mathrm{GPa} \tag{7}$$

and K is the contact pressure factor given by

$$K = 0.454 + 0.41\nu = 0.544. \tag{8}$$

Additionally, the GW plasticity index of the sample was calculated as follows:

$$\psi = \sqrt{\frac{\sigma_s}{\omega_c}} = 1.86. \tag{9}$$

It must be noted that if the face of the tip was assumed to have a roughness of 10 nm, the GW plasticity index can increase to a value as high as $\psi = 2.06$.

V. ANALYTICAL MODELING COMPARISON

The sample parameters were imported into the contact model presented by Kadin *et al.*,[23] which predicts the load-unload response of a rough surface. The model was formulated based on the assumption that each asperity in the contacting surface has a hemispherical tip that can permanently deform during a load-unload cycle. The contacting surface is imported into the model as a probability distribution function, and its load response is modeled by statistically summing the contributions of all of the contacting asperities.

The contact model of Kadin *et al.*[23] drew upon a set of empirical relations to describe the load-unload response of a single asperity in contact with a rigid flat. During loading, the load-interference relation for an elastic-plastic asperity is given by

$$W = 1.32W_c\left(\frac{\omega}{\omega_c} - 1\right)^{1.27} + 1, \tag{10}$$

where W_c is the critical load for elastic-plastic contact. During unloading, the force-interference relation for a single asperity is given as follows:

$$W = W_{max}\left(\frac{\omega - \omega_{res}}{\omega_{max} - \omega_{res}}\right)^{n_p}, \tag{11}$$

where ω_{res} is the residual interference that is caused by plastic deformation after a load-unload cycle and n_p is an exponential factor given by $n_p = 1.5(\omega_{max}/\omega_c)^{-0.0331}$, where ω_{max} is the maximum interference during loading.

VI. FEM MODELING OF FLAT PUNCH COMPRESSION

An explicit FEM modeling approach was used to simulate the flat punch compression of the SU-8 thin photoresist film. FEM is a robust computational modeling tool, which is particularly well-suited for resolving the physics of contact between complex geometries both qualitatively and quantitatively. This made it an ideal candidate for simulating the contact of a rigid flat punch against a real surface with a deterministic topography. Details about the type of FEM approach employed and the modeling procedure for simulating the experiment are now described.

A. The explicit FEM modeling approach

In this work, an explicit FEM modeling approach was employed using the computational tool ANSYS LS-DYNA. In general, there are two types of FEM methods—explicit and implicit—which utilize two different time integration techniques to treat the contact mechanics. The more traditional and well-known approach is the implicit FEM model, which applies a forward differencing technique with constant average accelerations. Suitable for transient contact events, the explicit FEM approach applies a central difference technique where a linear change in displacements is assumed. This approach is conditionally stable, which means it is stable unless the time step is less than a critical value. More details about this FEM approach can be found in works by the authors.[28,29]

B. FEM modeling procedure

The measured topography of the raised surface was imported into LS-DYNA, a commercial FEM solver, in order to simulate its normal load response when being loaded and unloaded against a rigid flat. The FEM solver was executed using a desktop personal computer with dual-core 3.2 GHz processors and 16 GB of random-access memory. The sur-

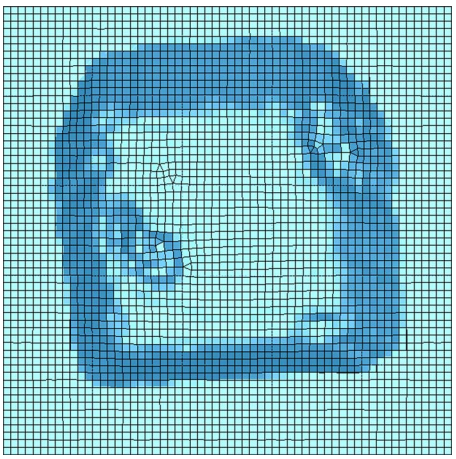

FIG. 4. (Color online) Surface grid of bottom raised square sample (top view).

face grid of the sample is shown in Fig. 4, while Fig. 5 shows the entire simulation domain. Although the raised surface in the sample had a thickness of $t=6.3$ μm, it was assumed that the deflection of the bulk material was negligible compared to the deflection of the asperities.

The bottom surface was specified with a piecewise linear plasticity material model[30] with the mechanical properties of SU-8 (see Table I). In order to be consistent with the rigid diamond indenter that was used in the flat punch experiments, the top surface was specified with a rigid body material model. Similar to the experiments, the simulated load-unload simulation was performed under a loading rate of 50 μN/s and an unloading rate of 20 μN/s with a maximum load of $W=1000$ μN.

1. FEM convergence test

The prediction of the FEM solver was tested for convergence by running a series of similar load-unload contact simulations with varying mesh sizes. The mesh sizes that were simulated contained 6948, 8028, 8993, 10 800, and 12 345 rectangular elements, respectively. In order to quantify the convergence of the FEM prediction, the predicted interference at maximum load ω_{max} was extracted from each simulation. Figure 6 shows the percent error between the predicted ω_{max} of the coarser grids compared with that of the finest, 12 345-element grid. It can be observed from this figure that the percent error decreases monotonically as the mesh size increases, which indicates the convergence of the solution.

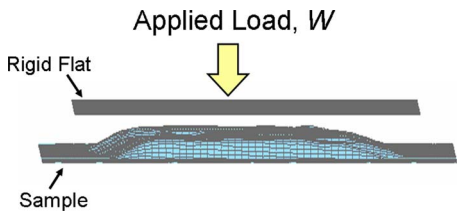

FIG. 5. (Color online) FEM simulation domain of the raised square sample and the rigid flat (side view).

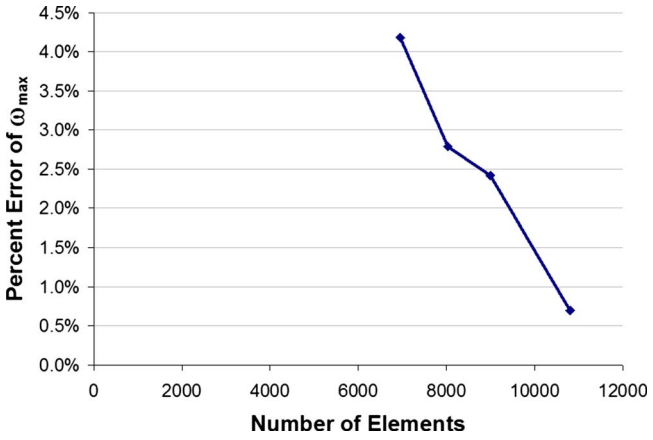

FIG. 6. (Color online) Percent error of ω_{max} between the coarsest grids and the finest 12 345-element grid.

2. FEM model used in present study

The FEM mesh that was observed for this study consisted of 10 800 elements, with 13 807 total nodes. Using the desktop personal computer described in Sec. VI B, this simulation took approximately 4 min to execute. The predictions from this simulation were used to directly compare to the experiment as well as to provide useful insight into the physics, which could not be obtained from experiment. As a direct comparison to experimental data, the predicted interference ω of the bottom (sample) surface was extracted at various applied loads throughout the simulated compression. In addition, the predicted distribution of von Mises stresses was also observed in order to determine the degree of plastic deformation that occurred. The von Mises stress is an equivalent stress, which is calculated from the principal stresses as follows:[31]

$$\sigma_0 = \sqrt{\tfrac{1}{2}[(\sigma_x-\sigma_y)^2+(\sigma_y-\sigma_z)^2+(\sigma_z-\sigma_x)^2+6(\tau_{xy}^2+\tau_{yz}^2+\tau_{xz}^2)]}, \tag{12}$$

where σ_x, σ_y, and σ_z are the normal stresses in each of the three Cartesian directions and τ_{xy}, τ_{yz}, and τ_{xz} are the shear stresses in each direction.

VII. RESULTS AND DISCUSSION

Figure 7 shows the predictions of the force-interference response from the FEM and analytical contact models compared to the measurements from the flat punch compression experiment. From observing the experimental results, it can be seen that the surface during unloading is more deformed than it was during the loading process, which confirms that the contact is elastic-plastic. With the exception of $3.5 \leq (\omega/\omega_c) \leq 4$, the FEM model of the load-interference response agrees with the experimental results with good accuracy.

It can be seen that the load-interference results from the FEM model predicted experimental data with good accuracy. Additionally, it can be observed that the analytical load-unload model by Kadin *et al.*[23] slightly overpredicted the surface deformation when compared to experiment. It must be noted, however, that the analytical solution would be closer to experiment if the roughness of the flat tip was taken

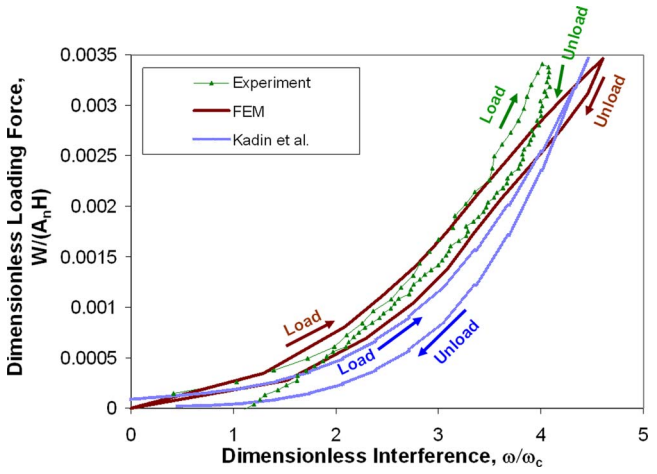

FIG. 7. (Color online) Predicted and experimental load-interference data for flat punch compression of the raised square.

into account. This change would be attributed to the effect of surface roughness on increasing the GW plasticity index ψ. A higher plasticity index would result in a decrease in predicted interference under a given load, thus causing the analytical predictions to match the experimental results more closely.

Because the FEM predictions provided a reasonable agreement with experimental results, it can be reasoned that the detailed modeling results from the FEM simulation can be accurately used to obtain quantitative insight into the experimental physics. Figures 8(a)–8(f) show the evolution of von Mises stress contours across the raised square during loading, while Figs. 9(a)–9(e) show the von Mises stress distribution during unloading. Since the areas of highest stress indicate where the surface is in contact with the rigid flat, these figures provide tremendous insight into the distribution of real contact area across the interface during compression. From Figs. 8(a)–8(f) it can be seen that at the lowest load, the highest stress is localized around the highest asperities and then forms a perimeter to encircle the raised square as the load is increased. Additionally, in all of the figures it appears that there are nonzero stresses in the noncontacting areas of the surface, which indicates that there is asperity interaction and a significant propagation of stress across the surface of the sample. As the surface is unloaded, it is interesting to observe that a significant amount of residual stress remains within the sample even as the applied load is decreased to 0 μN.

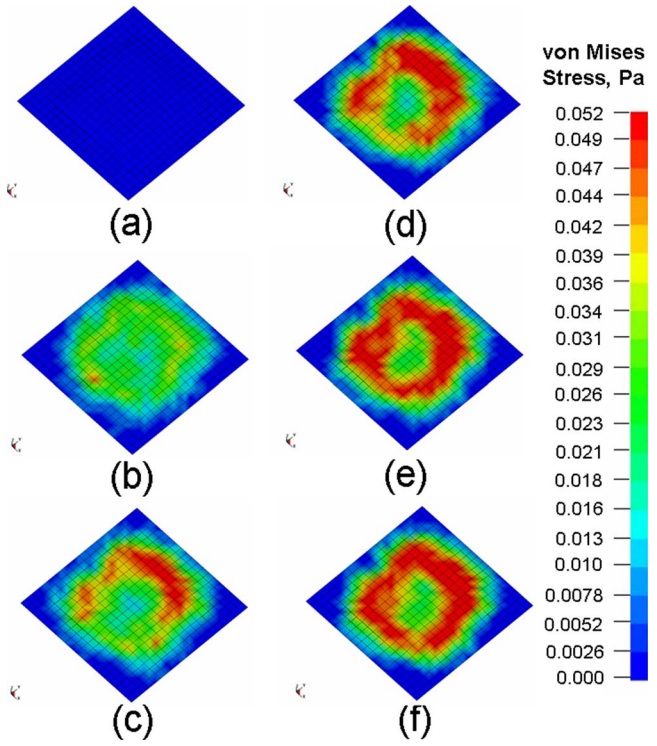

FIG. 8. (Color online) Evolution of the von Mises stress across the bottom (sample) surface during loading under loads of (a) $W=0$ μN, (b) $W=200$ μN, (c) $W=400$ μN, (d) $W=600$ μN, (e) $W=800$ μN, and (f) $W=1000$ μN.

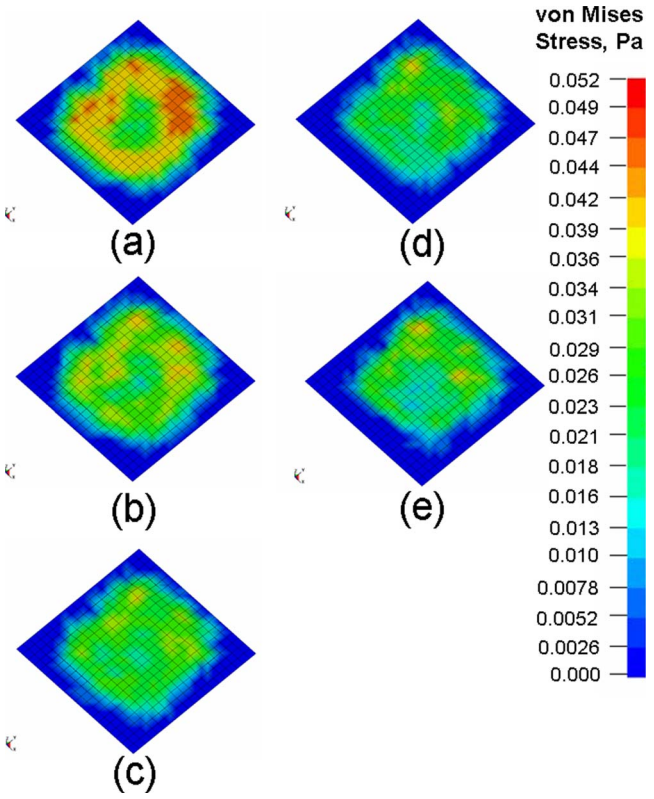

FIG. 9. (Color online) Evolution of von Mises stress across the bottom surface during unloading under loads of (a) $W=800$ μN, (b) $W=600$ μN, (c) $W=400$ μN, (d) $W=200$ μN, and (e) $W=0$ μN.

VIII. CONCLUSION

This study analyzed the normal loading of a SU-8 thin film raised square surface in order to evaluate both an analytical model and an FEM model against a thin film compression experiment. By performing nanoindentation with a flat diamond tip, it was possible to perform an asperity-scale flat punch compression test of a thin film region of known topography and mechanical properties. The results of the FEM simulation were found to compare well with the experimental compression data, while the analytical model slightly overpredicted the experimental results. Additionally, the FEM predictions were used in order to gain insight into the

intrinsic material behavior by observing the evolution of the von Mises stress distributions across the sample. From this study, the FEM simulation indicated the propagation of traverse stresses across the surface of the sample, as well as residual stresses in the surface during unloading.

This effort provides experimental data for the flat punch compression of a rough surface at the asperity scale. In comparing asperity-scale experimental contact results to modeling predictions, it was shown that FEM contact models that incorporate the actual deterministic topographies of the interacting surfaces have the capability of providing good insight into compression physics that cannot be gained from experiment. However, an interesting possibility for future research involves the investigation of experimental methods to observe the real contact area distribution in the contact of rough surfaces. The results of such research would provide an additional level of contact mechanics modeling validation.

ACKNOWLEDGMENTS

The authors gratefully acknowledge the support of the Alfred P. Sloan Foundation and the NSF CAREER award no. 0645124. The authors also thank Professor Michael Lovell from the University of Wisconsin at Milwaukee for comments on the FEM model. Lastly, the authors would like to thank the members of the Particle Flow and Tribology Laboratory (PFTL) at Carnegie Mellon University for their scholarly input in this work, namely, Joseph Bonivel, Venkata Jasti, Jeremiah Mpagazehe, Sarah Neyer, and Emmanuel Wornyoh.

[1]B. Bhushan, H. Liu, and S. M. Hsu, Trans. ASME, J. Tribol. **126**, 583 (2004).
[2]C. A. Morrow and M. R. Lovell, Trans. ASME, J. Tribol. **127**, 206 (2005).
[3]N. Tayebi and A. A. Polycarpou, J. Appl. Phys. **98**, 073528 (2005).
[4]C. F. Higgs III, E. J. Terrell, M. Kuo, J. Bonivel, and S. Biltz, Mater. Res. Soc. Symp. Proc. **991**, 2007.
[5]J. F. Luo and D. A. Dornfeld, IEEE Trans. Semicond. Manuf. **14**, 112 (2001).
[6]J. Seok, C. P. Sukam, A. T. Kim, J. A. Tichy, and T. S. Cale, Wear **254**, 307 (2003).
[7]C. F. Higgs III, S. H. Ng, L. Borucki, and S. Danyluk, J. Electrochem. Soc. **152**, G193 (2005).
[8]K. Komvopoulos, Wear **238**, 1 (2000).
[9]H. Li, B. Liu, W. Hua, and T.-C. Chong, J. Appl. Phys. **97**, 10P305 (2005).
[10]H. Tani, K. Goshi, T. Hamaguchi, and K. Suzuki, J. Appl. Phys. **99**, 08N104 (2006).
[11]W. Yan and K. Komvopoulos, J. Appl. Phys. **84**, 3617 (1998).
[12]C. Yang, U. Tartaglino, and B. N. J. Persson, Eur. Phys. J. E **19**, 47 (2006).
[13]A. Majumdar and B. Bhushan, Trans. ASME, J. Tribol. **113**, 1 (1991).
[14]G. Liu, J. Zhu, L. Yu, and Q. J. Wang, Tribol. Trans. **44**, 437 (2001).
[15]A. Martini, B. Escoffier, Q. Wang, S. B. Liu, L. M. Keer, D. Zhu, and M. Bujold, Tribol. Lett. **23**, 243 (2006).
[16]A. Martini, G. Velter, L. M. Keer, and Q. J. Wang, Tribol. Lett. **27**, 61 (2007).
[17]J. A. Greenwood and J. B. Williamson, Proc. R. Soc. London, Ser. A **A295**, 300 (1966).
[18]G. G. Adams and M. Nosonovsky, Tribol. Int. **33**, 431 (2000).
[19]J. I. McCool, Trans. ASME, J. Tribol. **122**, 496 (2000).
[20]R. L. Jackson and I. Green, Tribol. Int. **39**, 906 (2006).
[21]L. Kogut and I. Etsion, Tribol. Trans. **46**, 383 (2003).
[22]Z. Lestyan, K. Varadi, and A. Albers, Tribol. Int. **40**, 982 (2007).
[23]Y. Kadin, Y. Kligerman, and I. Etsion, J. Mech. Phys. Solids **54**, 2652 (2006).
[24]K. Kim, E. Nilsen, T. Huang, A. Kim, M. Ellis, G. Skidmore, and J.-B. Lee, Microsyst. Technol. **10**, 689 (2004).
[25]TriboIndenter User's Manual, Hysitron, Inc., Minneapolis, MN, 2003.
[26]J. I. McCool, Trans. ASME, J. Tribol. **108**, 380 (1986).
[27]W. R. Chang, I. Etsion, and D. B. Bogy, Trans. ASME, J. Tribol. **109**, 257 (1987).
[28]M. A. Kabir, M. R. Lovell, and C. F. Higgs, Tribol. Lett. **29**, 85 (2008).
[29]M. A. Kabir, V. K. Jasti, C. F. Higgs III, and M. R. Lovell, Proc. Inst. Mech. Eng., Part J: J. Eng. Tribol. **222**, 715 (2008).
[30]J. O. Hallquist, LS-DYNA Theory Manual, Livermore Software Technology Corporation, Livermore, CA, 1998.
[31]C. Srinivasa-Murthy, D. Wang, S. P. Beaudoin, T. Bibby, K. Holland, and T. S. Cale, Thin Solid Films **308–309**, 533 (1997).